Annual Letter Report

Pseudomorphic Semiconducting Heterostructures from Combinations of AlN, GaN and Selected SiC Polytypes: Theoretical Advancement and its Coordination with Experimental Studies of Nucleation, Growth, Characterization and Device Development

Supported under Grant #N00014-90-J-1427
Department of the Navy
Office of the Chief of Naval Research
Report for the period January 1, 1991–June 30, 1991

Robert F. Davis, Zlatko Sitar, Max W. H. Braun, and Larry Rowland
Materials Science and Engineering Department
North Carolina State University
Campus Box 7907
Raleigh, NC 27695-7907

June, 1991

REPORT DOCUMENTATION PAGE

Form Approved
OMB No 0704 0188

1. AGENCY USE ONLY (Leave blank)	2. REPORT DATE	3. REPORT TYPE AND DATES COVERED
	June, 1991	Semi-annual Letter 1/1/91-6/30/91

4. TITLE AND SUBTITLE Pseudomorphic Semiconducting Hetero-structures from Combinations of AlN, GaN and Selected SiC Polytypes: Theoretical Advancement and its Coordination with Experimental Studies

5. FUNDING NUMBERS

414s007---01
1114SS
N00179
N66005
4B855

6. AUTHOR(S)

Robert F. Davis

7. PERFORMING ORGANIZATION NAME(S) AND ADDRESS(ES)

North Carolina State University
Hillsborough Street
Raleigh,NC 27695

8. PERFORMING ORGANIZATION REPORT NUMBER

N00014-90-J-1427

9. SPONSORING/MONITORING AGENCY NAME(S) AND ADDRESS(ES)

Department of the Navy
Office of the Chief of Naval Research
800 North Quincy, Code 1513:CMB
Arlington, VA 22217-5000

10. SPONSORING/MONITORING AGENCY REPORT NUMBER

11. SUPPLEMENTARY NOTES

12a. DISTRIBUTION/AVAILABILITY STATEMENT

Approved for Public Release; Distribution Unlimited

12b. DISTRIBUTION CODE

13. ABSTRACT *(Maximum 200 words)*

The initial stages of growth of AlN and GaN on the Si (0001) face of α(6H)-SiC and the (0001) face of sapphire have been studied. The growth of both nitrides on the α(6H)-SiC substrates occurred on a thin (≈1 monolayer) of Si_3N_4. No significant surface chemical changes were observed when the films were grown on sapphire. The deposition of GaN on sapphire appeared to follow a Stranski-Krastanov mode of growth that on SiC showed characteristics of three-dimensional growth—possibly due to the Si_3N_4. The AlN grew on both substrates either layer-by-layer or, more likely, by the Stranski-Krastanov mode. The gas-source MBE for the growth of SiC-AlN-GaN heterostructures has been commissioned. Growth of single crystal (100) β-SiC on 3° off-axis Si(100) substrates at 1075°C has been successful. Two classes of computer codes have also been developed for theoretical modelling of pseudomorphic heterostructures of complex systems.

14. SUBJECT TERMS

pseudomorphic heterostructures, gallium nitride, aluminum nitride, gas-source molecular beam epitaxy

15. NUMBER OF PAGES

25

16. PRICE CODE

17. SECURITY CLASSIFICATION OF REPORT	18. SECURITY CLASSIFICATION OF THIS PAGE	19. SECURITY CLASSIFICATION OF ABSTRACT	20. LIMITATION OF ABSTRACT
UNCLAS	UNCLAS	UNCLAS	SAR

Table of Contents

I.	**Initial Morphology and Interface Chemistry During the Growth of GaN and AlN on α-SiC and Sapphire**	1
	A. Introduction	1
	B. Experimental Procedures	2
	Deposition System	2
	Film Growth	3
	XPS Analysis	4
	C. Results and Discussion	8
	Growth morphology	8
	Interface chemistry of the growth of GaN and AlN on SiC and sapphire	10
	D. Conclusions	13
	E. Future Research Plans	15
II.	**The Gas Source Molecular Beam Epitaxy of Silicon Carbide**	15
	A. Introduction	15
	B. Experimental Procedures	16
	C. Results	16
	D. Discussion	17
	E. Conclusions	20
	F. Future Plans/Goals	20
III.	**Development of Computational Codes for Investigating Pseudomorphic Semiconducting Heterostructures**	21
	A. Background	21
	B. Milestones for the First Phase	21
	C. Computer Codes	21
	Class 1	21
	Class 2	23
	D. Conclusions	24
IV.	**References**	24

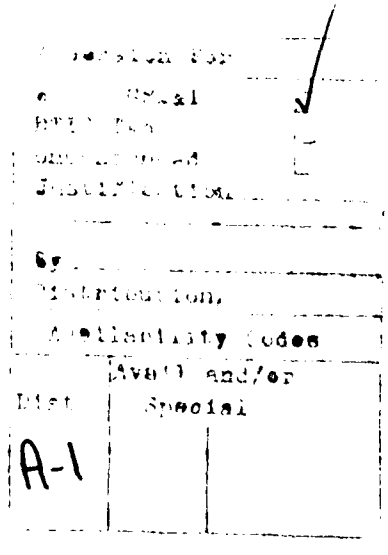

I. Initial Morphology and Interface Chemistry During the Growth of GaN and AlN on α-SiC and Sapphire

A. Introduction

Development and commercialization of LEDs and semiconductor lasers in the 70's generated much interest in the wide bandgap semiconductor GaN. Since it has a band gap of 3.45 eV (near UV region) at room temperature, and makes a continuous range of solid solutions with AlN (6.28 eV) and InN (1.95 eV), it is a promising material for UV as well as visible radiation. Gallium nitride also possesses two unique properties required in a semiconductor material to be used in fabricating transit-time-limited (IMPATT, etc.) microwave power amplifiers. It is predicted to have a large saturated electron drift velocity [1] which results in short transit times and thus allows the fabrication of high frequency devices. The other important property is the bandgap, which is more than twice that of GaAs and three times that of Si. Since pair-production threshold scales with the bandgap, then a GaN transit-time-limited device in reverse bias at high field would be able to operate at higher voltages. In power amplifiers, the power scales as the square of the voltage, thus GaN would have a significant advantage over Si or GaAs.

Bandgap engineering in the range of 1.95–6.2 eV can be achieved either by solid solutions or by layered structures of GaN, AlN and InN. The latter are favored for several reasons. As has been shown for the GaAs/GaAlAs system [2-5], optoelectronic devices using multi–quantum well structures instead of heterostructures exhibit lower threshold current density, lower non–radiative recombination rate, narrower emission spectra and reduced sensitivity to temperature.

However, bulk wavers of either material are not available, thus they must be grown heteroepitaxially. So far, sapphire has been the most commonly used substrate, despite the huge lattice mismatch. The quality of the heteroepitaxially grown films depends on two key issues, the lattice mismatch between the substrate and film, and the relation of their respective surface energies.

Three different growth regimes are clearly distinguished. The first one is layer-by-layer (or two dimensional) growth, in which the deposited film completes one monolayer of coverage, then the second, the third, etc. This type of growth is observed, when the substrate surface energy, σ_S, exceeds the sum of the surface energy of the overgrowth, σ_O, and the interfacial energy, σ_i (i.e. $\sigma_S \geq \sigma_O + \sigma_i$). The second regime is so called Stranski-Krastanov growth, in which the first layer completely covers the surface of the substrate, while the subsequent layers form islands of deposited material. This type of growth satisfies the same equation as layer-by-layer growth, but islanding occurs due to high strain energy, which

arises due to the lattice mismatch. The third regime is three dimensional growth, in which the material immediately forms islands on the surface. This type of growth occurs when $\sigma_S \leq \sigma_O + \sigma_i$.

Surface energies of solids are hard to measure. They can be accurately predicted for some metals, while the calculations for compounds give rather erroneous results. The closest approximation for the covalently bonded materials is the summation of the energy of the unsatisfied bonds per unit area of the surface [6]. However, bond energies can not be determine accurately either.

As such, one cannot determine easily which substrate would be best suited for the growth of a certain material, e.g., GaN or AlN, since there are too many variables which cannot be determined with sufficient accuracy. However, one can design a rather time consuming experiment which answers the question regarding the initial stages of growth.

Such an experiment consists of several sequences of growth of 0.5 to 1 monolayer of material in each sequence. After each growth step the sample is analyzed either by Auger spectroscopy or XPS. The growth steps are repeated until a total of five to ten monolayers have been grown.

It is known, that electrons of a particular energy travel in solids a certain distance without loosing their energy. This distance is called the escape depth. When they are passing through a material, their flux decreases exponentially. Since low energy electrons (a few 100 eV) have a very short escape depth (usually in the order of a few monolayers), they are a sensitive measuring tool for the characterization of the growth mode of very thin layers. If the substrate is excited with high energy electrons or photons which easily penetrate the grown film well beyond the escape region for characteristic electrons, one can consider the substrate as a source of an electron flux I_0. If a film is deposited in small steps, the electron flux of characteristic substrate lines decreases with the film thickness. The dependence of the electron flux on film thickness can give us the information regarding the initial stages of growth. A calculated plot of the Auger signal from the substrate with respect to film thickness is shown in Figure 1 [7] for all three types of growth.

B. Experimental Procedures

Deposition System. The growth system was a commercial Perkin-Elmer 430 MBE system modified as described below. It consisted of three major sections: a load lock (base pressure $\approx 5 \times 10^{-8}$ Torr), a transfer tube (base pressure $\approx 1 \times 10^{-10}$ Torr) which was used to degas the substrates, and the growth chamber (base pressure $\approx 5 \times 10^{-11}$ Torr). Knudson effusion cells (20 cc) with BN crucibles and Ta wire heaters were charged with 47 g of 7N pure gallium or 5 g of 6N pure aluminum.

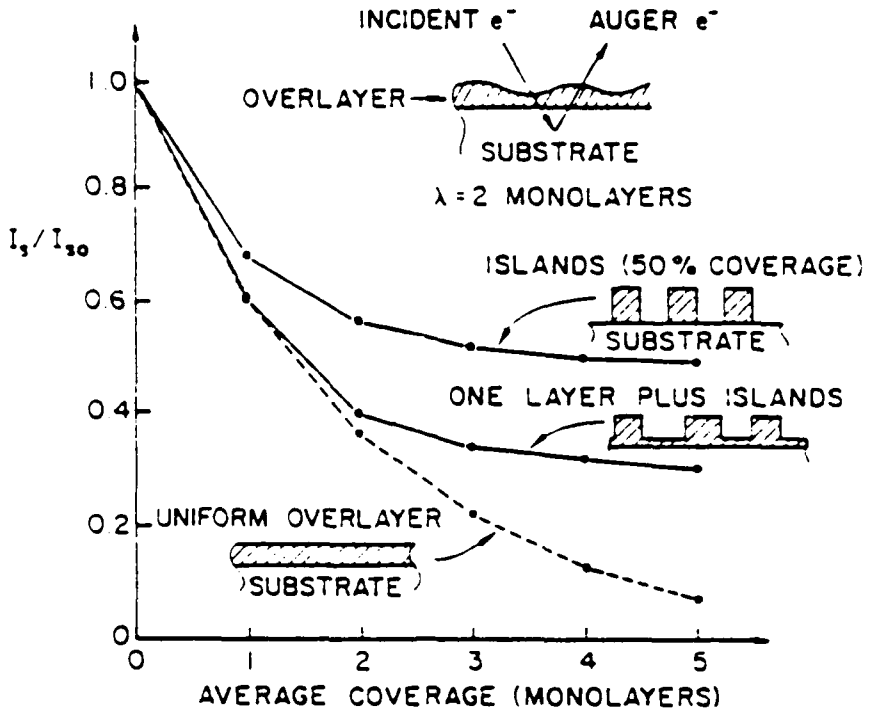

Figure 1. Extinction curves for characteristic substrate electrons as a function of average coverage of an overlayer.

Films of GaN and AlN could not be produced within the experimental conditions of this study using molecular nitrogen. Therefore an ECR plasma source was designed, constructed and commissioned [8] in order to efficiently activate/dissociate molecules of this gas. This unique source has the advantage of fitting inside the 2.25 inch diameter tube of the source flange cryoshroud. Using this design, the source–to–substrate distance was minimized which increased the flux density at the substrate. A similar plasma source was not commercially available at the outset of this effort. Some important parameters of the ECR source are given in the Table I. Ultra–high–purity nitrogen, further purified by a chemical purifier, was used as the source gas. The flow rate was regulated by a variable leak valve and was normally ≈5 sccm which resulted in a chamber pressure of 1×10^{-4} Torr.

Film Growth. Growth studies were conducted on (0001)-oriented α(6H)-SiC and (0001)-oriented epitaxial quality sapphire wafers, both of which have a hexagonal structure. All substrates were cleaned to remove organic and metallic contaminants using the following sequence of chemicals, temperatures and times: 1:1:5 solution of HNO_3:H_2O_2:H_2O at 75°C for 5 min, DI chemicals, temperatures and times: 1:1:5 solution of HNO_3:H_2O_2:H_2O at 75°C

Table I. Some parameters of the NCSU-ECR nitrogen plasma source.

Overall source diameter	57 mm
Plasma diameter	23 mm
Microwave frequency	2.45GHz
Microwave power	0–100 W
Peak magnetic flux	1.05 kG
Nitrogen ion current density at 50 W	
• at the source	$\approx$1 mAcm^{-2}
• at the substrate	150–200 μAcm^{-2}
Start pressure	1×10^{-4} Torr
Minimum operation pressure	1×10^{-5} Torr

for 5 min, DI water rinse for 1 min, 1:1:5 solution of $HCl:H_2O_2:H_2O$ at 75°C for 5 min and DI water for 5 min and finally 1:10 solution of $49\%HF:H_2O$ for 5 min and DI water for 5 min. All substrates were then mounted on a standard 3 inch molybdenum block with indium which provided both good adherence and thermal contact.

The substrates underwent an initial low temperature ($\approx$70°C) outgasing in the load lock followed by slow heating in the transfer tube to a maximum of 700°C with a dwell time of 30 min at this temperature. After cooling, the samples were introduced into the growth chamber and examined by reflection high energy electron diffraction (RHEED) using a 10 kV beam. The resulting RHEED patterns on both the α-SiC and sapphire substrates showed Kikuchi lines indicative of good crystalline quality.

Prior to growth, the substrates were heated to the desired deposition temperature and subsequently exposed to a flux of plasma activated nitrogen species for about 5 min. Following the stabilization of temperatures and fluxes, a thin layer of GaN or AlN was grown. The growth conditions are summarized in Table II. After the growth was completed, the gallium or aluminum cell and the substrate were cooled, while the nitrogen source remained active. This source was turned off and the growth chamber returned to UHV conditions once the substrate temperature was below 400°C.

XPS Analysis. XPS (X-ray photoelectron spectroscopy) was performed on the cleaned substrates prior to deposition and on the grown films after each deposition step, in which about half of a MBE growth chamber to an UHV analytical chamber. XPS spectra were

Table II. Growth conditions.

Nitrogen pressure	$1x10^{-4}$ Torr
Microwave power	50 W
Gallium temperature	900°C
Aluminum temperature	1120°C
Substrate temperature	600°C
Thickness grown/deposition	~0.2 nm
Number of deposition cycles	6
Total number of monolayers grown	~5

obtained with a Riber Mg/Al XPS X-ray source and a Riber MAC II cylindrical electron analyzer. Spectral data were acquired by an IBM PC-AT running software developed at NCSU.

For study of the AlN growth, Mg Kα X-rays (1253.6 eV) were used to obtain spectra. For GaN growth, both the Mg and Al (1486.6 eV) anodes were used. The reason for alternating the X-ray sources for the examination of GaN is due to the fact that the Ga Auger electron emission occupies a large region of the spectrum between 0 and 1000 eV, and covers up certain XPS photoemission peaks of interest. Changing the X-ray energy, used for XPS, shifts the Auger emission lines on an intensity vs. binding energy plot for the difference in the energy of the X-ray photons, while the positions of the XPS photopeaks remains the same. The effect of changing the energy of X-rays is illustrated in Figure 2. Figure 2(a) is a wide-scan survey spectrum of GaN on sapphire obtained with the Mg X-ray anode, showing both substrate and film photopeaks and the Ga_{LMM} Auger emission cluster, which covers about 300 eV wide band of the spectrum. Figure 2(b) is a similar survey spectrum of GaN on SiC using the Al X-ray source; this spectrum shows that the Ga Auger emission has been shifted by an amount equal to the energy difference between the two sources (233 eV). Owing to the positions of the Ga Auger emission, the Mg anode was used for examining the O_{1s} and N_{1s} photopeaks, while the Al anode was used for examining the C_{1s}, Si_{2s}, Al_{2p} and Ga_{3d} peaks.

For the study of GaN, the Si_{2s} photopeak at 153 eV was used, rather than the more commonly used Si_{2p} peak, again because of interference from Ga emission. The Ga_{3p} peak at 107 eV lies very close to Si_{2p} at 103 eV, and overwhelms the Si_{2p} emission as the Ga signal grows during deposition. The Si_{2s} peak is also near another Ga photopeak (Ga_{3s} at 160 eV) but is located farther from the nearby Ga peak than the Si_{2p} peak is from its own Ga neighbor.

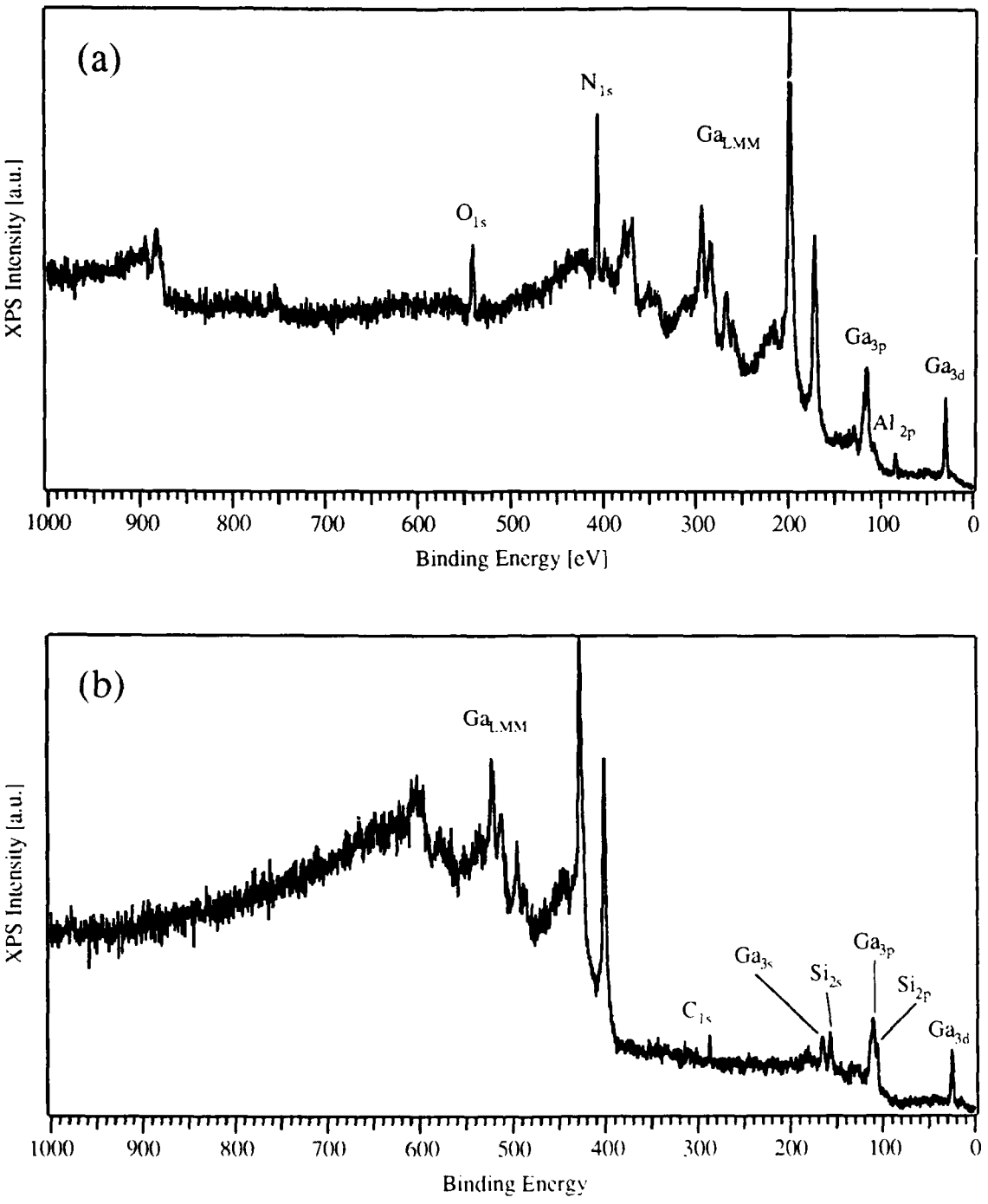

Figure 2. XPS survey spectra of GaN films: (a) Sapphire substrate, Mg X-ray source. (b) SiC substrate, Al X-ray source.

The areas of the substrate peaks obtained after each deposition were calculated, compared to the areas of the peaks from the virgin substrate, and finally plotted vs. film thickness. Results were compared with a theoretical curve for layer-by-layer growth.

Electron escape depths were obtained from Figure 3 [7]. The data show, that the escape depth is energy dependent with a broad minimum centered around 100 eV. The escape depth is relatively insensitive to the material traversed by the electrons. Since XPS photoelectrons of C_{1s}, Si_{2s} and O_{1s} have considerably different binding energies, the energies of escape electrons differ as well. The energy of an escaped electron equals the incident X-ray photon energy minus the electron binding energy. Thus electrons with higher binding energy acquire less kinetic energy when being excited with the same kind of X-rays. Switching of the anodes from Mg to Al has also been taken into account. The energies of escaped photoelectrons and respective escape depths are summarized in Table III.

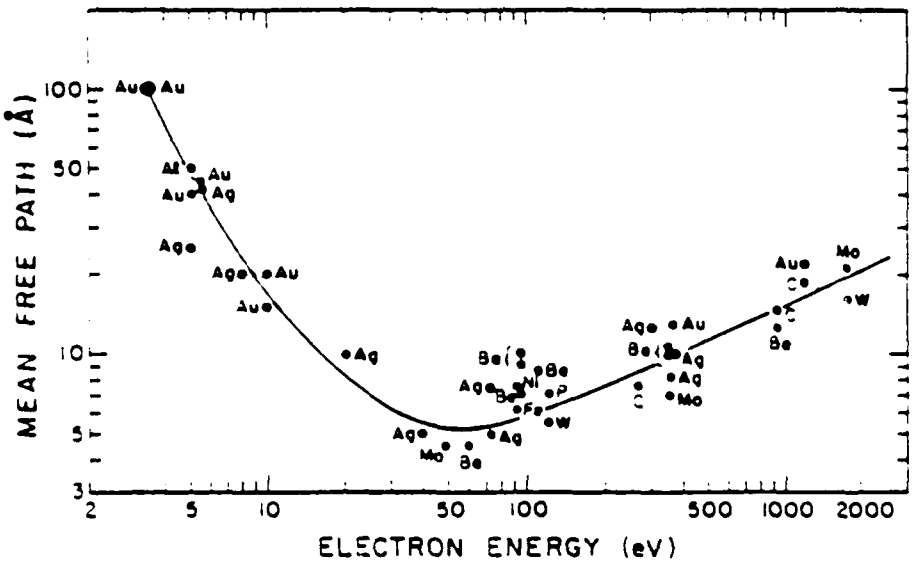

Figure 3. Universal curve for electron mean free path (escape depth).

Table III. Photoelectron energies and their escape depths.

	O_{1s}	C_{1s}	Si_{2s}
Photon Energy [eV]	1254	1487	1487
Binding Energy [eV]	531	283	152
Kinetic Energy [eV]	723	1204	1335
Escape Depth [Å]	12±1	18±1	18±1

Si_{2s} and C_{1s} peak intensities were monitored during the growth on SiC substrates and O_{1s} peak was examined during the growth on sapphire.

The binding energy values of the XPS photopeaks were referenced to that of the particular peak for each film which was expected to be the most invariant. Such referencing of the peak locations minimizes the effects of the analyzer characteristics and specimen charging. For the films grown on SiC, the C_{1s} peak was set at a typical value for SiC [9,10,11], 283.0 eV, and the other peaks were referenced to that value. For the films grown on sapphire substrates, the N_{1s} values of 397.0 for GaN [11,12] and 397.3 for AlN [11,13] were used. For the clean sapphire substrates prior to deposition the photopeaks were referenced to the average value for O_{1s} observed during the rest of the deposition.

C. Results and Discussion

Growth morphology. Figures 4 and 5 show plots of relative substrate peak intensities vs. film thickness obtained during the growth of GaN and AlN, respectively. Both figures contain also theoretical curves representing layer-by-layer growth calculated at two escape depths, 18 (O_{1s}) and 13 (C_{1s},Si_{2s}) Å. The two curves correspond to the growth on sapphire and SiC, respectively.

A perusal of Figure 4 shows, that the substrate peak intensity diminishes faster at the growth of GaN on SiC than on sapphire (compare O_{1s} to C_{1s} and Si_{2p} signals). This is most likely partially due to faster initial nucleation process on SiC, and partially due to the formation of a thin silicon nitride layer at the interface. (The evidence for that will be discussed later.) This reasoning also agrees with the subsequent behavior of the plot where the O_{1s} signal decreases rapidly (once initial nucleation occurs) with the same derivative as the Si_{2p} and C_{1s} signals at the very beginning of the growth. Furthermore, an earlier study of the growth rate of GaN on different substrates did not indicate a substantial difference between the growth rates on SiC and sapphire, within our experimental conditions.

Although one would expect, from common sense, the same behavior for Si_{2s} and C_{1s} peaks from SiC, they behave differently. The C_{1s} peak intensity shows a faster initial drop and also saturates at a much lower value. This can also be explained by the formation of a thin layer of silicon nitride. Since the Si-face of the SiC substrates was used, a silicon nitride layer formed on the surface. This produced a buried carbon layer which now resided even farther under the Si. The difference in the initial intensity drop approximately corresponds to the formation of one monolayer of silicon nitride.

All three curves assume a more gradual behavior after the initial rapid drop. The derivatives of the C_{1s} and Si_{2s} signals in this region are considerably lower than the

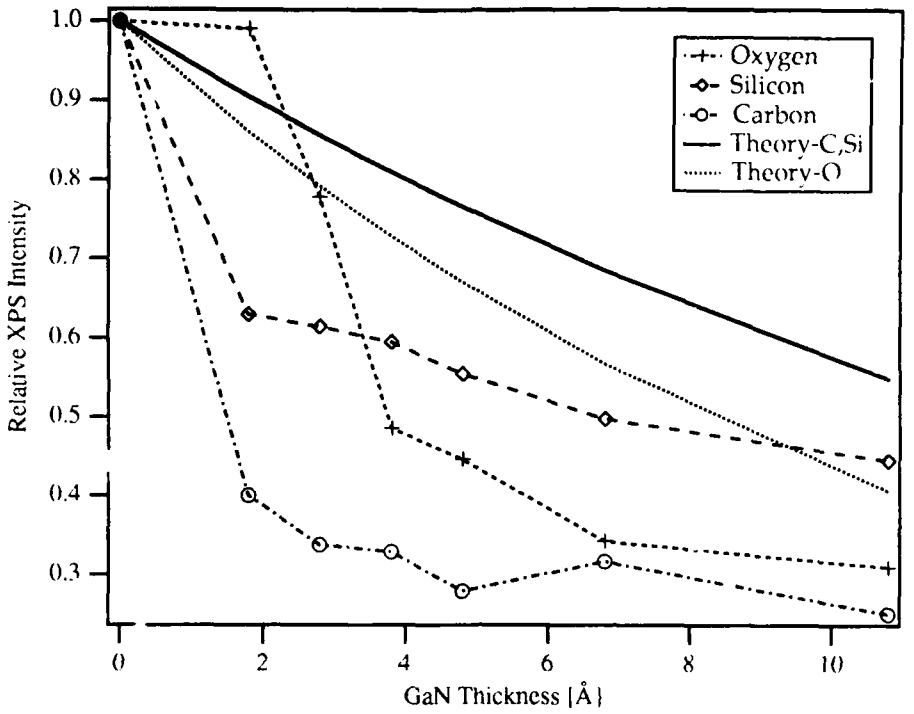

Figure 4. Change of XPS photoelectron intensity during the growth of GaN on α(6H)-SiC and sapphire.

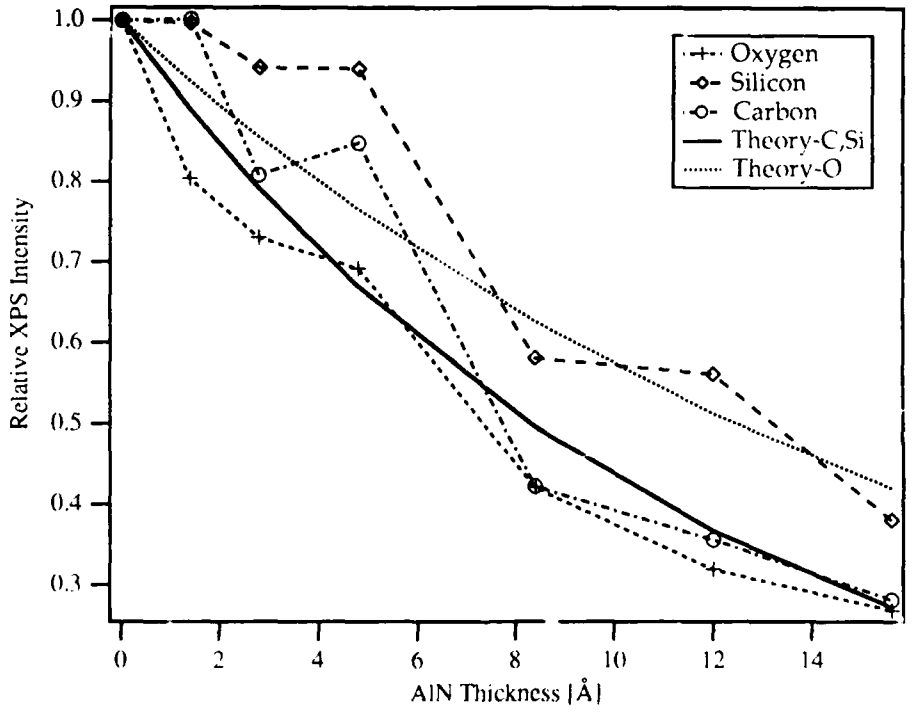

Figure 5. Change of XPS photoelectron intensity during the growth of AlN on α(6H)-SiC and sapphire.

derivative of the corresponding theoretical curve, while the derivative of the O_{1s} signal exhibits a closer match to its theoretical curve. However, none of the experimental curves resembles the corresponding calculated curves for layer-by-layer growth.

The growth of GaN on sapphire appears to follow the Stranski-Krastanov mode, while the growth on SiC shows some characteristics of three dimensional growth, although one would expect from the lattice mismatch a smoother growth on SiC than on sapphire. At present, it is not clear, whether or not this is solely due to formation of a thin interfacial layer of silicon nitride.

Figure 5 shows the change in XPS substrate peak intensities acquired during the growth of AlN. A few differences and similarities with the respect to Figure 4 can be seen quickly. In this case, experimental data do not show a rapid initial decrease and they resemble respective theoretical curves much better. This may indicate, that AlN does indeed grow layer-by-layer or perhaps in a more forgiving Stranski-Krastanov regime, where the complete coverage of a few monolayers is obtained. This is in agreement with several reports, that GaN films are effected beneficially, when grown on an AlN buffer layer previously deposited on sapphire.

The decrease in the Si_{2s} and C_{1s} peaks shows more closely related behavior than in Figure 4. The carbon signal decreases faster initially and levels off at a lower value than Si_{2s} peak. This indicates that a thin film of silicon nitride was formed also in this case.

Interface chemistry of the growth of GaN and AlN on SiC and sapphire. XPS was also used to characterize the chemical state of the substrates, interfaces and the growing films during the MBE deposition of GaN and AlN. Analysis of the cleaned substrates prior to deposition revealed the presence of very small amounts of carbon and oxygen surface contamination.

The binding energy values obtained with reference to a particular peak for the growth series of GaN and AlN on sapphire and on α(6H)-SiC are listed in Tables IV and V.

With the exception of the Si_{2p} peak from SiC, none of the substrate XPS signals were altered significantly due to the film deposition. Over the course of AlN deposition on sapphire, the Al_{2p} peak shifted slightly to a lower value as the AlN covered the Al_2O_3, but the shift was a subtle one, and the overall peak shape did not change measurably.

The sequence of the Si_{2p} peaks acquired between deposition steps during the growth of AlN on α(6H)-SiC is shown in Figure 6. The initial Si_{2p} signal from the clean substrate was a symmetrical peak characteristic of clean SiC. With the first AlN growth step, significant shouldering of the peak appeared on the high binding energy side, indicating the presence of a more highly oxidized state of the silicon. This shoulder persisted throughout the film deposition process and remained as the SiC component and the overall the Si intensity diminished with film growth. Gaussian curve fitting analysis was applied to the most intense,

Table IV. Binding energies of XPS photoelectrons measured during the GaN growth on sapphire and α(6H)-SiC.

Growth Step	0	1	2	3	4	5	6
On sapphire:							
Al_{2p}	74.0	73.8	73.6	73.4	73.7	73.4	73.4
O_{1s}	531.0*	531.3	531.1	531.0	531.2	531.0	530.9
Ga_{3d}	-	19.3	19.2	19.0	19.2	19.1	19.2
N_{1s}*	-	397.0	397.0	397.0	397.0	397.0	397.0
On α(6H)-SiC:							
Si_{2s}	152.1	152.2	152.2	152.2	152.2	152.2	152.2
C_{1s}*	283.0	283.0	283.0	283.0	283.0	283.0	(83.0
Ga_{3d}	-	19.9	19.9	20.0	19.9	20.0	20.0
N_{1s}	-	397.7	397.6	397.7	397.5	397.6	397.7

* Values set as reference

Table V. Binding energies of XPS photoelectrons measured during the AlN growth on sapphire and α(6H)-SiC.

Step	0	1	2	3	4	5	6
On sapphire:							
Al_{2p}	75.0	75.0	75.0	74.8	74.5	74.2	74.1
O_{1s}	532.0*	532.2	532.1	532.0	531.9	531.8	531.8
N_{1s}*	-	397.3	397.3	397.3	397.3	397.3	397.3
On α(6H)-SiC:							
Si_{2p}	100.9	101.0	101.0	101.1	101.1	101.0	101.1
C_{1s}	283.0	283.0	283.0	283.0	283.0	283.0	283.0
Al_{2p}	-	NSP	NSP	NSP	74.0	74.0	74.1
N_{1s}	-	397.6	397.6	397.5	397.3	397.3	397.4

* Values set as references, NSP = no significant peak.

shouldered peak, obtained at the first growth step, to resolve the position of the high binding energy component. The results of curve fitting are shown in Figure 7.

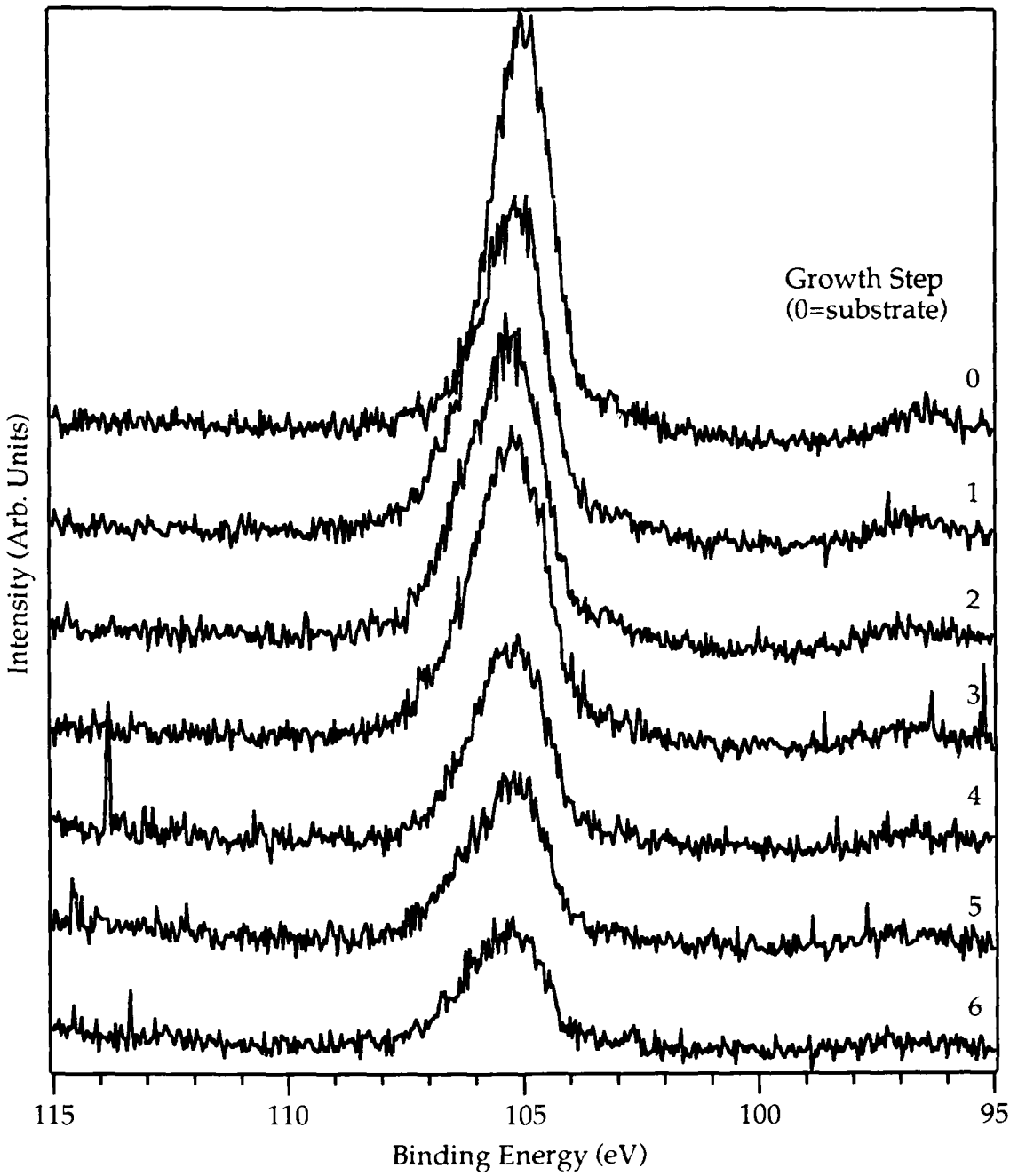

Figure 6. Si_{2p} photoemission as a function of AlN growth on SiC. Shoulder developed on the high binding energy side was due to the formation of Si_3N_4.

By means of Gaussian curve fitting, the high binding energy shouldering was found to be primarily due to a single component shifted 1.4 eV from the main SiC peak. This component has been attributed to the formation of Si_3N_4 during the initial stages of AlN growth. This behavior shows that the Si-face of SiC initially undergoes nitridation. The films are thus actually deposited on a thin (probably just one monolayer) layer of Si_3N_4.

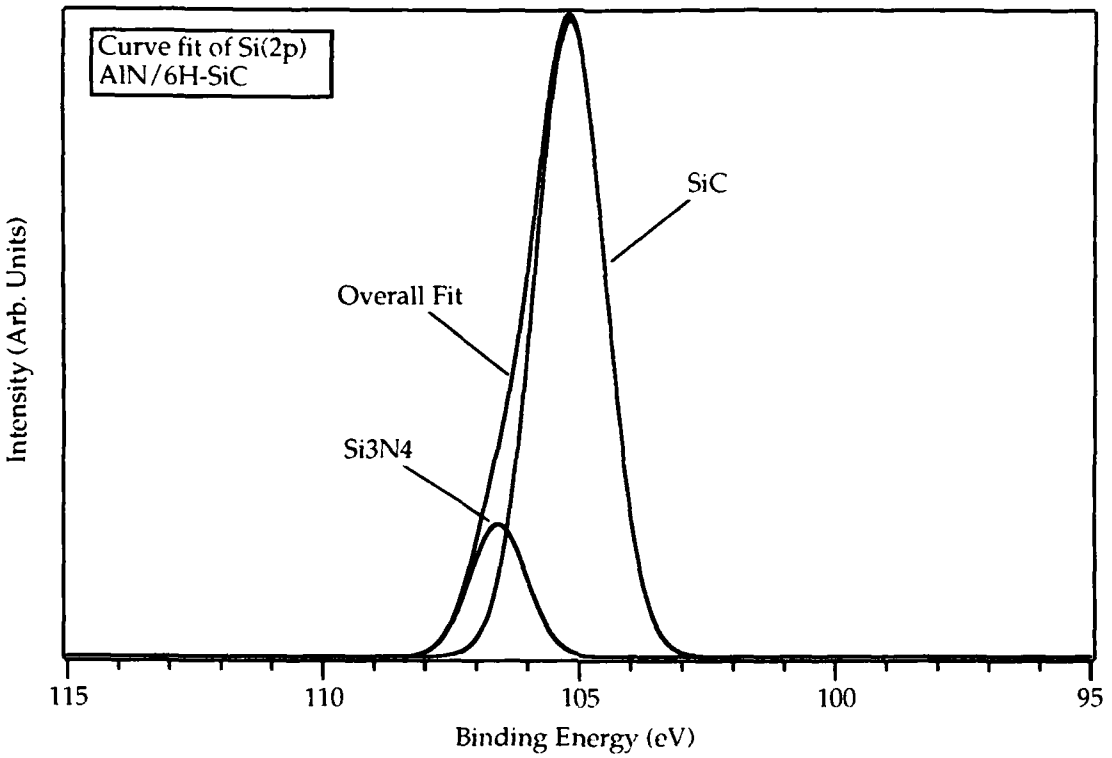

Figure 7. Curve fit of Si_{2p} photopeak from initial stages of AlN deposition, showing Si_3N_4 component shifted 1.2 eV from SiC binding energy.

The sequence of Si_{2p} peaks acquired between deposition steps during the growth of GaN on α(6H)-SiC is shown in Figure 8. A similar conclusion could not be made for the growth of GaN on SiC, although there is little reason to expect that in this case a completely different chemistry initially occurred at the interface. We believe, that the effect could not be seen, since spectra obtained during the growth of GaN, show lower peak-intensities and a poorer signal-to-noise ratio. The close proximity of the Ga_{3s} peak on the high energy side, as shown in Figure 2, could have obscured the evidence of the silicon nitride formation as well.

The film elements Ga, Al, and N exhibited no significant changes in chemistry, except for the slight shift of the Al_{2p} peak from AlN growth on sapphire as the Al_2O_3 gave way to AlN. Thus the XPS analysis indicates that no significant chemical reactions occurred between the growing films and the substrates other than the formation of small amounts of interfacial Si_3N_4 during the initial stages of growth on SiC.

D. Conclusions

The initial stages of growth of AlN and GaN on SiC and sapphire substrates have been studied. The information on the interface morphology and chemistry has been obtained.

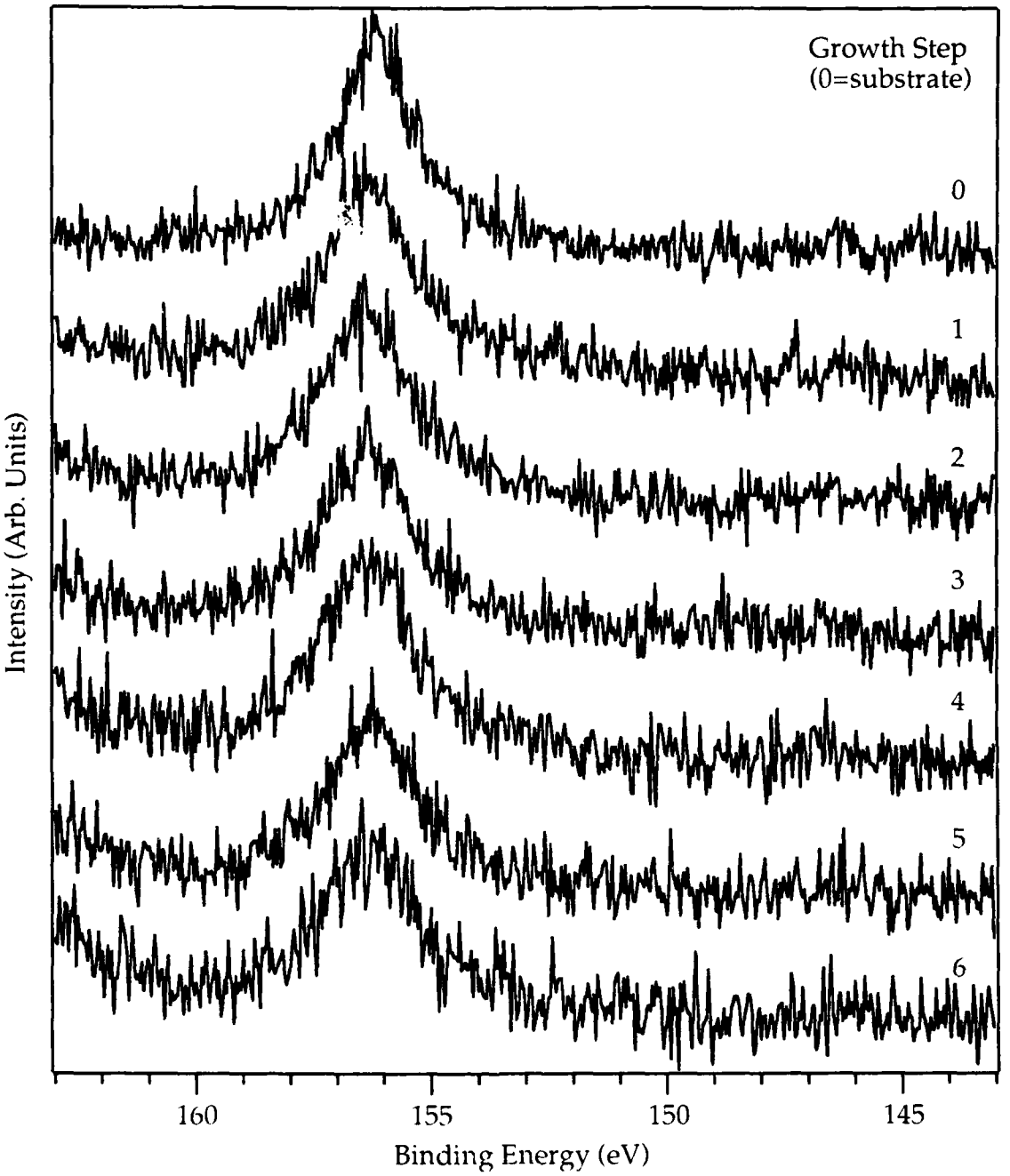

Figure 8. Si_{2s} photoemission as a function of GaN growth on SiC.

The growth of both nitrides on the Si (0001) face of the SiC substrates formed a thin layer of Si_3N_4. The evidence for Si_3N_4 formation was obtained from the study of Si oxidation states and from the study of substrate peak intensity dependence on the film thickness. No significant chemical changes were observed when the films were grown on sapphire.

A faster GaN nucleation was observed on SiC, while AlN apparently nucleated on both substrates equally well.

The deposition of GaN on sapphire appeared to follow the Stranski-Krastanov mode of growth. By comparison, the growth of GaN on SiC showed some characteristics of three dimensional growth, although one would expect from the lattice mismatch a smoother growth on SiC than on sapphire. At present, it is not clear, whether or not this is solely due to formation of thin interfacial layer of Si_3N_4 or not.

The study of AlN showed that it does grow on both substrates by a layer-by-layer mode or maybe in the more forgiving Stranski-Krastanov regime, where the complete coverage of a few monolayers is obtained.

E. Future Research Plans

The research concerned with the growth of AlN, GaN and their layered structures in the MBE system will be continued. Since the primary goals are the improvement of the quality the materials, and the growth of p-type GaN and AlN, the short term research will be devoted to few more interface studies. Magnesium will be used as the dopant for both compounds. A Hg UV light source is going to be used for further doping and interface studies. Having achieved the quality and desired electrical properties, all efforts will be focused toward the growth of structures for simple optoelectronic devices.

II. The Gas Source Molecular Beam Epitaxy of Silicon Carbide

A. Introduction

Beta SiC, the lone zincblende (cubic) polytype in the Si-C system, has the potential for employment in specialized electronic applications which can use its attractive physical and electronic properties such as wide band gap (2.2 eV at 300K) [14], high breakdown electric field (2.5×10^6 V/cm) [15], high thermal conductivity (3.9 W/cm °C) [16], high melting point (3103K at 30 atm) [17], high saturated drift velocity (2×10^7 m/s) [18], and small dielectric constant (9.7) [19].

Growth of SiC has traditionally been performed on Si substrates due to the lack of availability of high-quality SiC substrates. The recent development of high-purity single-crystal wafers of hexagonal α(6H)-SiC by Cree Research, Inc. has made growth on these substrates more feasible, and future research is planned on these substrates. Growth on silicon has progressed over the years despite large mismatches in the coefficients of thermal expansion and the lattice parameters between the two materials. To date, chemical vapor deposition (CVD) has been primarily used as the method of choice for growth of β-SiC on Si. However, the high growth temperature used and the relative lack of control of growth thickness and unintentionally introduced doping species found in SiC produced by CVD have given an impetus to the development and construction of a gas source molecular beam

epitaxy (GSMBE) system for growth and doping of SiC. Molecular beam epitaxy allows for precise control of growth parameters and minimization of sample contamination during deposition. Parameters such as growth thickness and dopant concentration can thus be controlled at the monolayer level and reproducibly obtained using this technique.

Growth using the system has commenced, with experiments performed to date concerned with growth of β-SiC on off-axis Si, due to the relative abundance of Si substrate material. In the following sections preliminary results obtained for SiC growth on off-axis Si (100) substrates, including growth of monocrystalline β-SiC are presented. In addition, the future research using α(6H)-SiC substrates provided by Cree Research is described.

B. Experimental Procedures

Growth studies were performed on 3° off-axis (100) heavily arsenic-doped Si wafers (ρ=.002.-.004 Ω-cm). All substrates were cleaned prior to growth in the following manner: H_2SO_4 at 70°C for 5 min, DI water rinse for 1 min, 1:1 solution (by volume) of 50% H_2O_2 and NH_4OH at 70°C for 5 min, DI water rinse for 1 min, BOE etch at room temperature for 5 min, and DI water rinse for 2 min. After cleaning, the samples were secured in a SiC-coated graphite sample holder and placed in the load lock. After the load lock reached a pressure of 2×10^{-6} torr or less, the samples were then transferred to the growth chamber. The base pressure of the system prior to growth is typically 1×10^{-9} torr. A gas-source molecular beam epitaxy system described in detail in previous reports was used for the deposition.

Prior to growth, samples were heated in UHV conditions for about 5 min at the desired growth temperature to remove any surface contaminants. Source gases (Si_2H_6 and C_2H_4) were then simultaneously introduced into the system to initiate film growth. Flow rates of Si_2H_6 have been varied from 0.2 to 0.4 sccm, while flow of C_2H_4 has been kept at 2.0 sccm in all but one experiment. The pressure during growth has typically been 6×10^{-5} torr. Growth temperatures have been varied to date from 1025°C to 1125°C.

The chemical composition and depth profiles of the samples were obtained using a JEOL JAMP-30 scanning Auger microprobe. Samples which showed a 1:1 Si to C ratio from Auger results were then examined by reflection high-energy electron diffraction (RHEED) with an incident beam energy of 10 keV to determine the crystal structure and an estimate of film quality.

C. Results

Growth at 1075°C using the flow rates of 2.0 sccm C_2H_4 and 0.4 sccm Si_2H_6 for 90 min produced a monocrystalline β-SiC film. Auger spectra from the surface showed the presence of a surface oxide from atmospheric exposure after growth. Once the surface oxide was removed via Ar sputtering, the sample was found to be stoichometric SiC. Figure 9 (a) shows

the Auger depth profile from a sample grown under the conditions just noted. The film shows 1:1 stoichometry to a thickness of around 700Å. The oxygen level shown on the depth profile is a typical background level for the Auger system. Examination of a monocrystalline β-SiC film previously grown on (100) Si using CVD as a standard for comparison gave a resultant Auger depth profile nearly identical to that found in the first 700Å of the film shown in the figure.

Other experimental conditions attempted to date have resulted in a Si-rich stoichometry as shown by Auger analysis. A typical example of this is shown in Figure 9(b), which is a sample grown at 1025°C with 1.0 sccm C_2H_4 and 0.2 sccm Si_2H_6 for 90 min. It is interesting to note that results from growth at 1125°C using 2.0 sccm C_2H_4 and 0.4 sccm Si_2H_6 did not produce a 1:1 SiC ratio as occurred at 1075°C.

RHEED analysis of the SiC sample show the film to have the expected cubic crystal structure and to be monocrystalline. RHEED patterns (Figure 10) were taken for different orientations of the SiC film. Slight streaking of the pattern indicates that the film has a fairly smooth morphology and is of relatively good quality. The (110) reflection (Figure 10(b)) shows some evidence of twinning in the film. Films of β-SiC grown by chemical vapor deposition (CVD) typically show a large density of defects including twins [20]. Optical and scanning electron micrographs of all films to date show a pitted surface region which is likely due to preferential evaporation along {111} planes in the Si substrates [21]. Transmission electron microscopy of this film is planned in the near future.

D. Discussion

Auger and RHEED results indicate the presence of epitaxial β-SiC on Si at 1075°C. However, the same conditions at a higher temperature produce a Si-rich film as indicated by Auger. In addition, a film grown at 1125°C with a 10:1 C/Si source ratio (2.0 sccm C_2H_4 and 0.2 sccm Si_2H_6) for 90 min was also Si-rich. The use of a greater C/Si ratio did result in a greater amount of C in the grown film, but still did not result in a 1:1 Si- to C-ratio. This is an unexpected result, as an increase in temperature should correspond to an increase in the decomposition of C_2H_4. Apparently the decomposition of Si_2H_6 is also improved.

The possibility that Si could be diffusing into the growing film, leading to a Si-rich film, comes to mind. However, carburization of the Si substrate (0.5 sccm C_2H_4 for 0 min) followed by growth at 1125°C at 2.0 sccm C_2H_4 and 0.2 sccm Si_2H_6 for 90 min resulted in a film with a similar Si:C ratio and a thickness similar to that grown without the carburization step. Carburized layers grown by CVD, where Si is supplied by diffusion from the substrate, are typically 5-12 nm in thickness when grown in 5 min as the temperature is increased from

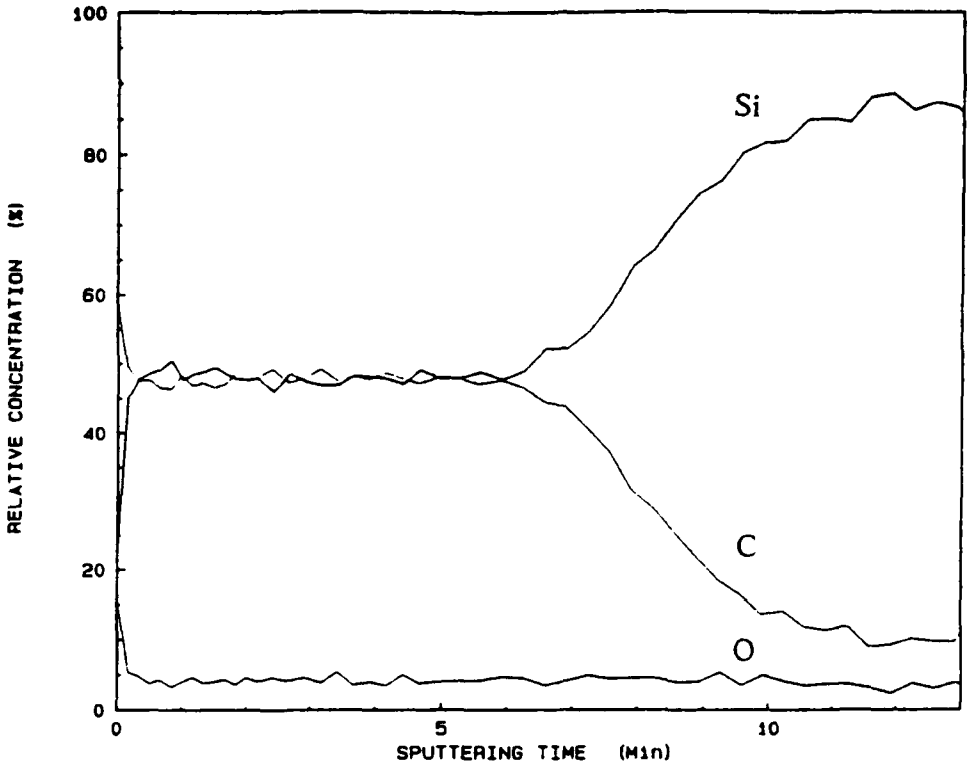

Figure 9a. Auger depth profile of SiC sample grown at 1075°C.

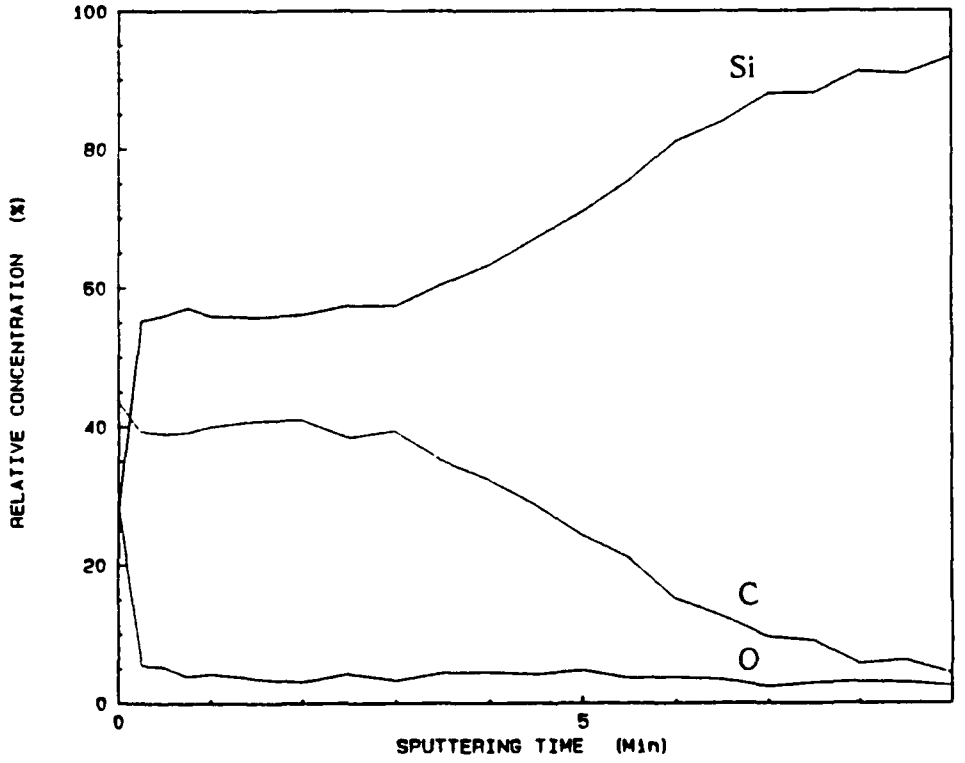

Figure 9b. Auger depth profile of SiC sample grown at 1025°C.

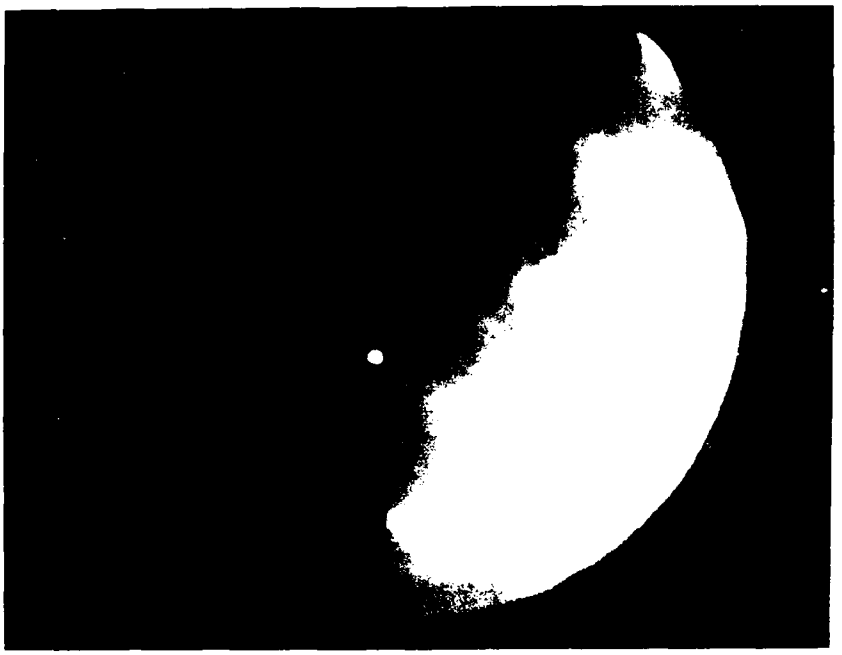

Figure 10a. β-SiC RHEED pattern from (1000) reflection.

Figure 10b. β-SiC RHEED pattern from (110) reflection.

25°C to 1360°C [22]. Si-rich layers grown to date in the MBE system are typically much thicker; the thickness of the film shown in Figure 9(b) is approximately 80 nm thick. This is undoubtedly too thick for Si diffusion from the substrate into the growing film to play a major role in the Si-rich character of the films grown at higher temperatures.

Pitting of the sample surface during growth is quite likely related to preferential evaporation of Si from the Si substrate at dislocation cores [21]. These pits appear rectangular or square in shape, and are believed to actually be pyramids bounded by {111} planes. These pyramids are similar to those initially seen for carburization of Si surfaces for SiC growth [23]. Silicon samples heated under MBE conditions at temperatures where significant evaporation occurs (750°C or higher for (100) Si wafers [24]) typically show this pitted morphology. Silicon films grown as low as 800°C using 1.0 sccm disilane in this MBE system during initial testing of the growth system showed this pitted morphology, as observed by optical microscopy. Suppression of formation of these pitted regions may be possible with the proper choice of growth conditions and substrate cleaning methods.

E. Conclusions

The gas source MBE growth system designed and built for growth of SiC films and SiC/AlN, GaN/AlN and SiC/AlN and GaN solid solutions and superlattices is now operational. Growth of stoichiometric β-SiC *(100) on Si (100) substrates has been achieved.* Preliminary results from Auger and RHEED analyses obtained on samples grown in this system indicate that heteroepitaxial growth of β-SiC on off-axis (100) Si substrates can be obtained under the conditions of 1075°C, 6×10^{-5} torr, 2.0 sccm C_2H_4 and 0.2 sccm Si_2H_6 for 90 min. Other conditions, including growth at higher temperatures, have yet to result in stoichiometric SiC films. Further work is necessary to optimize the growth parameters and to characterize the grown films.

F. Future Plans/Goals

Further analysis including transmission electron microscopy and electrical measurements of these films will be employed to characterize the grown films in greater detail. Further growth experiments are ongoing to determine the optimum flow rates of the gas sources and the growth temperatures for growth of β-SiC on Si. Results of this research will be described in the next report.

In the near future, growth on the Si (0001) face of α-SiC (6H) substrates provided by Cree Research will commence. In addition, doping of SiC films grown on SiC substrates will be performed using Al from an MBE effusion cell as the p-type dopant and N obtained from the electron cyclotron resonance (ECR) plasma decomposition of N_2 as the n-type dopant. In addition, growth will be attempted using an ECR source from ASTeX, Inc. for plasma

decomposition of C_2H_4 and CH_4 in order to lower the growth temperature. These SiC films will be characterized using TEM, RHEED, Auger, and secondary ion mass spectrometry (SIMS).

III. Development of Computational Codes for Investigating Pseudomorphic Semiconducting Heterostructures

A. Background

The basic system under investigation is a materials system constructed of layers of atoms of different crystalline substances. Usually one of the materials consists of a pre-existing slab of material (the substrate), while the second substance is grown on the first, to form a heterostructure. Several variables can be introduced to characterize the system, for example, the number of atomic layers ("thickness") of the overgrowth, the ratio of lattice parameters of the overgrowth and substrate substances, assuming a specific choice of structures, and the orientation with which the overgrowth grows on the substrate, expressed as the angle between specific lattice directions in the overgrowth and substrate crystals [25]. Additionally, the overgrowth and substrate may alternate to form a superlattice [26,27].

The study examines the conditions under which given materials will form stable or metastable heterostructures, the form of these heterostructures, and the properties of the resulting systems.

B. Milestones for the First Phase

i) Implementation of existing two-dimensional finite element programs modelling these materials structures [28].

ii) Extension to 3 dimensions.

iii) Extension of the code in ii) to include:

a) a superlattice system, by the inclusion of periodic boundary conditions in the third dimension,

b) atomistic overgrowth-substrate interaction.

(iv) Static relaxation of a fully atomistic many-body (embedded atom method, or Stillinger-Weber potentials).

v) Molecular dynamic simulation to study temperature effects and the calibration of many body potentials at regimes different from essentially static bulk behavior.

C. Computer Codes

Two classes of programs were developed during this time.

Class 1. Overgrowth and substrate systems were modelled on the following assumptions:

i) The overgrowth is treated as an island which experiences a potential derived from the substrate. The latter is expressed as two-dimensional Fourier series, truncated after a few orders. The total energy then depends on the details of the overgrowth and substrate structures, and the values of the Fourier coefficients of the potential.

ii) To allow compound semiconductors to be modelled, the overgrowth components are allowed to experience different substrate potentials. (This is a new generalization, not included in earlier models of this type).

The above assumptions together form the "Rigid Model," from which an optimum lattice parameter and orientational relationship may be obtained, which minimize the overgrowth-substrate interaction energy.

The Rigid model is implemented in the code MULTIMIS. The code a) plots the overgrowth-substrate interaction contributions as a function of position, using the CA-DISSPLA package [29] on FLYER; b) calculates and plots the interaction energies as a function of lattice parameter ratio and orientation, from which the optimal values can be directly inferred.

This code has been completed. An additional assumption introduces an improved model:

> By allowing the overgrowth to deform homogeneously, strain energy is included in the interaction energy, and the effect of a thickening overgrowth can be modelled. Optimal configurations minimize the energy subject to orientation as well as strain, and allow the prediction of critical thicknesses, beyond which the overgrowth-substrate system is unstable in a given configuration.

This homogeneous strain — or pseudomorphic — model is implemented in a code PSEUDO.

Types of output produced by PSEUDO include minimized total interfacial energies and separate misfit and elastic energies for a range of orientations and lattice parameter ratios, including the interfacial energies in non-deformed systems. Output data for graphical display in the form of 3-dimensional wire or contour diagrams, or sectional curves are produced by PSEUDO.

This code was still being tested and optimized in January, and the following problems still have to be overcome:

i) Convergence on a global minimum is still slow, and is not always achieved. This instability arises from generalization of the program to allow description of multiple-component compound semiconductors and the change from IMSL version 9 to IMSL version 10 [30]. The latter did not include the minimization routines

previously used, and parameters suitable for the new routine (BCONF) still need to be optimized.

ii) A visualization program to allow rapid interpretation of the results and selection of energetically favored configurations (the present version is called PHASE) is yet to be sufficiently generalized to match the generalizations included in PSEUDO.

It is intended that development of these programs will continue, and optimized for the CRAY.

The output from PSEUDO is necessary as input for the finite element suite whose completion marks the achievement of the first milestone in the project. The finite element programs need to be generalized in a similar manner as the MULTIMIS and PSEUDO programs to allow different atoms in the overgrowth to experience different potentials in the presence of the substrate.

Class 2. In order to provide values for both elastic constants and Fourier coefficients used in the Class 1 models, development of atomistic simulation codes based on the following principles were begun.

Principles:

The interaction between atoms in the materials system is described by interatomic potentials of embedded atom (method) type [31]. This formation is essentially an empirical form of density functional theory. The later is implemented for example in the package DMOL [32] recently tested on the CARAY at North Carolina Supercomputing Center.

Covalent compound semiconductors are described in terms of a modified embedded atom method of the type developed by Baskes, Nelson and Wright [33] in which bond directionality has been included in the formalism. Special potentials can benefit calibration by computer runs of the DMOL code.

A skeletal molecular dynamics code written with the collaboration of Dr. Joe Beeler of the Department of Materials Science and Engineering at NCSU was completed in Decembe. 1990. This program conformed to an embedded atom potential of the first type. During December an in early January the program was generalized to include potential and force terms due to directional bonds according to the modified embedded atom method. The key potential and force subroutines were vectorized by using a neighbor cell linked list which is highly efficient. Full testing however, was not completed; thus no objective performance figures can be given. Still to be included are the necessary subroutines to produce elastic constants and potential parameters, and appropriate periodic boundary conditions.

This molecular dynamics code, when fully completed, will yield a number of codes which together address the fourth and fifth milestones in the original grant proposal, and additionally provide input parameters for the Class 1 codes.

D. Conclusions

The resources were used to contribute to progress in the study of pseudomorphic semiconducting heterostructures. The program MULTIMIS has been completed, while PSEUDO and a molecular dynamics program based on an embedded atom formalism adapted to the description of covalent structures are well advanced.

While the research effort has temporarily moved to other computer facilities due to the completion of the sabbatical term of Dr. Braun, the research will once again return to NCSU during 1992, when supercomputer resources will be applied for once more.

All publications arising from research using these computer codes will gratefully acknowledge the contribution to this research made by this grant of resources by NCSC.

IV. References

1. K. Das and D. K. Ferry, Solid-State Electron. **19**, 851 (1976).
2. W. T. Tsang, Appl. Phys. Lett. **39**, 786 (1981).
3. M. G. Burt, Electron. Lett. **19**, 210 (1983).
4. P. Davson, G. Duggan, H. I. Ralph, and K. Woodbridge, Superlattices and Microstr. **1**, 173 (1985).
5. N. Holonyak, Jr., R. M. Kolbas, R. D. Dupuis, and P. D. Dapkus, IEEE J. Quantum Electron. QE **16**, 170 (1980).
6. A.W. Adamson, *Physical Chemistry of Surfaces*, 5th ed. John Wiley and Sons, Inc., N.Y., 1990.
7. L.C. Feldman and J.W. Mayer, *Fundamentals of Surface and Thin Film Analysis*, North-Holland, N.Y.
8. Z. Sitar, M. J. Paisley, D. K. Smith, and R. F. Davis, Rev. Sci. Instr. **61**, 2407 (1990).
9. F. Bozso, L. Muehlhoff, M. Trenary, W.J. Choyke, and J.T. Yates, Jr., J. Vac. Sci. Technol. A **2**, 1271 (1984).
10. P.A. Taylor, M. Bozack, W.J. Choyke, and J.T. Yates, Jr., J. Appl. Phys. **65**, 1099 (1989).
11. NIST X-Ray Photoelectron Spectroscopy Database, version 1.0, NIST Standard Reference Database 20. National Institute of Standards and Technology, Gaithersburg, MD, 1989.
12. J. Hedman and N. Mårtensson, **22**, 176 (1980).
13. A.D. Katnani and K.I. Papathomas, J. Vac. Sci. Technol. A **5**, 1335 (1987).
14. H. P. Philipp and E. A. Taft, in *Silicon Carbide, A High Temperature Semiconductor*, edited by J. R. O' Connor and J. Smiltens (Pergamon, New York, 1960), p. 371.
15. W. von Muench and I. Pfaffender, J. Appl. Phys. **48**, 4831 (1977).
16. E. A. Bergemeister, W. von Muench, and E. Pettenpaul, J. Appl. Phys. **50**, 5790 (1974).
17. R. I. Skace and G. A. Slack, in *Silicon Carbide, A High Temperature Semiconductor*, edited by J. R. O'Connor and J. Smiltens (Pergamon, New York, 1960), p. 24.
18. W. von Muench and E. Pettenpaul, J. Appl. Phys. **48**, 4823 (1977).
19. S. Nishino, Y. Hazuki, H. Matsunami, and T. Tanaka, J. Electrochem Soc. **127**, 2674 (1980).
20. C. H. Carter, Jr., R. F. Davis, and S. R. Nutt, J. Mater. Res. **1**, 811 (1986).
21. J. T. Glass, Y. C. Wang, H. S. Kong, and R. F. Davis, in *Heteroepitaxy on Silicon: Fundamentals, Structures, and Devices*, edited by H. K. Choi, H. Ishiwara, R. Hull, and R. J. Nemanich (Mat. Res. Soc. Symp. Proc. **116**, Pittsburgh, PA 1988), pp. 337-349.
22. Y. Ito, Thin Solid Films, **106** (3), 1 (1983).
23. A. Addamiano and J. A. Sprague, Appl. Phys. Lett. **44**, 525 (1983).

24. D. J. Robbins, A. J. Pidduck, A. G. Cullis, N. G. Chew, R. W. Hardeman, D. B. Gasson, C. Pickering, A. C. Daw, M. Johnson, and R. Jones, J. Cryst. Growth **81**, 421 (1987).
25. van der Merwe, J. H., Phil Mag **45** (1982) 127, 145, 159.
26. Matthews, J. W. and A. E. Blakeslee, J. Cryst. Growth **27** (1974) 118.
27. Sitar, Z., M. J. Paisley, D. K. Smith and R. F. Davis, Rev. Sci. Instr. **61** (1990) 2407.
28. Braun, M. W. H., "Epitaxy on substrates with hexagonal lattice symmetry," D.Sc. thesis, University of Pretoria, (1987).
29. CA-DISSPLA, Computer Associates, graphical subroutine package.
30. IMSL, International Mathematical and Statistical Library.
31. Daw, M. S., and M. I. Baskes, Phys. Rev. B **29** (1984) 6443.
32. DMOL, Biosym Technologies.
33. Baskes, M. I., J. S. Nelson and A. F. Wright, Phys. Rev. B. **40** (1989) 6085.